Desalination and Water Treatment
www.deswater.com
doi: 10.1080/19443994.2015.1119740

57 (2016) 21428–21436
September

Taylor & Francis
Taylor & Francis Group

Solar photocatalytic activity of indium sulfide nanocrystal and degradation of the tetracycline by In_2S_3

Cuiling Ai[a,b,*], Qian Wang[a], Yingjie Lei[b,c], Xiangwen Shao[a]

[a]*Fujian Provincial Key Laboratory of Photocatalysis-State Key Laboratory Breeding Base, College of Civil Engineering, Fuzhou University, 2 Xue Yuan Road, University Town, Fuzhou, Fujian 350108, China, Tel. +86 059122865361; emails: aicuiling@163.com (C. Ai), 340020773@qq.com (Q. Wang), 28028860@qq.com (X. Shao)*
[b]*Shaanxi Key Laboratory of Comprehensive Utilization of Tailings Resources, Shangluo University, 10 Bei Xin Street, Shangluo, Shaanxi 726000, China, Tel. +86 02260215678; email: yingjlei@163.com (Y. Lei)*
[c]*Department of Chemistry and Chemical Engineering, Tianjin University of Technology, 391 Binshui Xidao, Xiqing District, Tianjin 300384, China*

Received 7 April 2015; Accepted 4 November 2015

ABSTRACT

Nanocrystalline β-In_2S_3 was prepared by reacting $In(NO_3)_3$ with thioacetamide through hydrothermal method at 120°C for 12 h. The size and morphology of In_2S_3 photocatalyst were characterized using X-ray diffraction (XRD), scanning electron microscope (SEM), transmission electron microscopy (TEM), and Brunauer–Emmett–Teller (BET) surface area analysis. The band gap energy was measured using Kulbeka–Munk function and the electronic state of the prepared In_2S_3 was determined by X-ray photoelectron spectroscopy. The photocatalytic activity of the prepared sample was investigated by the photocatalytic degradation with 20 mg/L of the tetracycline (TC) under natural sunlight as a source of irradiation. The results showed that the synthesized In_2S_3 matches completely with the cubic phase of β-In_2S_3 with a surface area of 95.6726 m^2 g^{-1}, and the photocatalytic activity for the degradation of TC under natural sunlight irradiation was excellent followed with first-order kinetics and the complete removal could be within 30 min, which suggests that the prepared photocatalyst has the potential to degrade the antibiotics.

Keywords: Hydrothermal method; β-In_2S_3; Heterogeneous photocatalyst; Tetracycline degradation; Natural sunlight

1. Introduction

In recent years, considerable attention has been focused on the possibility of combining heterogeneous catalysis with solar technologies to achieve the degradation or mineralization of organic and inorganic pollutants present in water and wastewater [1]. Heterogeneous solar photocatalysts effectively utilize the energy from the sunlight, a renewable energy, for the photocatlytic reactions that can potentially reduce the treatment costs [2].

Typically, semiconductor powders have been extensively studied as photocatalysts over the past five decades, and In_2S_3 has attracted a great deal of attention due to its high photocatalytic activity, nontoxicity, photostability, chemical and thermal stability, low cost, and favorable optoelectronic properties [3]. It is

*Corresponding author.

well known that In_2S_3 occurs in nature as three crystallographic forms namely α-In_2S_3 (defect cubic structure, stable up to 693 K), β-In_2S_3 (defect spinel structure, stable up to 1027 K), and γ-In_2S_3 (layered hexagonal structure, stable above 1027 K) [4]. Among the three distinct forms, β-In_2S_3 is an *n*-type semiconductor with a band gap of 2.0–2.3 eV and is a potential candidate for solar cell [5], photocatalyst [6], photocatalytic hydrogen production [7], and optoelectronic [8] applications because of its defected spinel structure. The defected spinel structure is obtained in either cubic or tetragonal form.

In general, the photocatalytic activity of the In_2S_3 depends on several factors such as crystalline phase, crystal size, and specific surface area as well as on other factors, such as production capacity of electron–hole pair, separation efficiency of the photogenerated charge pair, and the transfer efficiency to compounds adsorbed on the In_2S_3 surface. In addition, the photoactivity of In_2S_3 also depends on the preparation method, thermal treatment, concentration of the pollutant, and concentration of the photocatalyst.

Numerous synthesis methods have already been reported by researchers to fabricate In_2S_3 with a variety of morphologies, such as hydrothermal [9], solvent thermal [10], chemical bath deposition [11], laser-induced synthesis [12], microwave synthesis route [13], and sonochemistry [14] of indium organic or inorganic salts. Different precursors have been employed for the synthesis of In_2S_3 nanoparticles such as indium nitrate [$In(NO_3)_3$] [15], indium acetylacetonate [16], and indium chloride ($InCl_3{\cdot}4H_2O$) [17]. Numerous research works have been conducted to obtain the different structure and morphology nanocrystals, such as hollow microsphere [18], and 3D flower-like morphology [17]. But the reports are scarce on the photocatalytic degradation studies using In_2S_3 for organic pollutants using solar light as a source of irradiation.

Thus the paper is focused to investigate the photocatalytic activity of β-In_2S_3 synthesized through hydrothermal method using $In(NO_3)_3$ as a precursor. The In_2S_3 samples were characterized with various analytical characterization techniques for their phase, morphology, elemental composition, surface properties, electronic configuration, optical property, and band gap energy. Furthermore, photocatalytic activity of the synthesized In_2S_3 photocatalysts was evaluated by degrading TC under natural solar light irradiation. In addition, the experimental photocatalytic degradation data were fitted with first-order kinetics to determine the degradation mechanism.

2. Experimental

2.1. Materials

Indium nitrate (99.9%) and tetracycline were procured from Aldrich, thioacetamide (99%) from Sinopharm Chemcial Reagent and anhydrous ethanol from Tianjin Fuchen Chemical Reagent. All chemicals were of analytical grade and used as received without any further purification.

2.2. Synthesis of indium sulfide nanoparticles

Synthesis of nanocrystalline In_2S_3 by hydrothermal method between indium nitrate and thioacetamide was performed in a glass beaker. Here, thioacetamide serves as a sulfur source. A certain amount of thioacetamide was added into a certain amount of $In(NO_3)_3$ solution under vigorous stirring (5:12 molar ratio of In:S). The reaction is vigorous in nature; finally, the colorless transparent solution was obtained. Eighty milliliters of the solution was then transferred into a 100-ml high pressure reactor and heated at 120℃ for 12 h. After the hydrothermal treatment, the suspension turned to orange color and then to orange-yellow color. The resulting In_2S_3 precipitate was cooled down to room temperature naturally and harvested by centrifugation at 8,000 rpm for 5 min and thoroughly washed with 10 mL of anhydrous ethanol. The washing step was repeated for three times and after every washing step, the solvent was removed by centrifugation. This ensures the complete removal of the possible remaining cations and anions. After washing, the obtained In_2S_3 orange-yellow powder was dried at 60℃ for 24 h and grinded in the agate mortar.

2.3. Characterization

The In_2S_3 samples were analyzed for their crystallite phase with powder X-ray diffraction (XRD) (Philips X'Pert Pro MPD X-ray diffractometer, Holland) using CoKa ($\lambda = 0.178901$ nm) radiation operating at 40 kV and 30 mA for the angle of diffraction 2θ between 5° and 95° with scan rate of 0.02 s^{-1}. Scanning electron microscope (SEM) (HITACHI S-4800, Japan) and transmission electron microscope (TEM) (Tecnai G2 F20 S-TWIN 200KV, FEI, the United States) were used to investigate the morphology and microstructure of the photocatalyst. Brunauer–Emmett–Teller (BET) surface area, pore volume, and Barret–Joyner–Halenda (BJH) pore size distribution based on nitrogen adsorption–desorption isotherms were analyzed with ASAP2020 M+C surface area and porosity system (the United States). Prior to surface

area analysis, the samples were degassed at 120°C for 5 h under nitrogen atmosphere. X-ray photoelectron spectra (XPS) were obtained with ESCALAB 250 instrument of Thermo Scientific (the United States) using monochromatic AlKa radiation (225 W, 15 mA, 15 kV). The binding energy (BE) of adventitious C 1*s* (284.9 eV) was used as reference. UV–vis diffuse reflectance spectroscopy of the samples was performed through Shimadzu SHIMADZU UV-2450 scanning spectrophotometer (Japan) using $BaSO_4$ as a reference. From the absorption edge, the band gap values were calculated by the extrapolation method.

2.4. Photocatalytic experiments

All photoreaction experiments were carried out in a photocatalytic reactor system, which consists of a quartz glass reactor vessel, a magnetic stirrer, and other parts. Photocatalytic activity of the In_2S_3 sample was evaluated by the photocatalytic degradation of TC under sunlight. The experiments were carried out in a batch reactor of 50 mL capacity with a working volume of 40 mL (initial concentration of TC = 20 mg L^{-1}) under continuous stirring in the presence of natural sunlight by adding 2.5 g L^{-1} of the photocatalyst. For each run, the reaction suspensions were freshly prepared. The sunlight intensity during the experiment was between 10,000 and 200,000 lx. Since the photocatalytic reactions occur in the adsorbed phase, dark experiments were carried out prior to photocatalytic experiments to substantiate the possibility of parallel removal of TC by adsorption. Additional control experiments were carried out with zero photocatalyst condition to ensure the degradation was only due to presence of photocatalyst. Three replicates of all experiments were performed at identical conditions to check the reproducibility of the experimental results. The analytical samples were drawn out at regular intervals (10 min), immediately centrifuged at 12,000 rpm for 5 min, and then filtered to remove the catalyst and analyzed for residual concentration of TC using an UV–vis spectrophotometry (WFZ UV-2000, Unico) at 357 nm to understand the TC degradation. The degree of mineralization of TC during photocatalytic experiment was estimated from the amount of total organic carbon (TOC) before and after photocatalytic degradation process using Elementar High TOC Analyzer (the United States).

3. Results and discussion

3.1. Structure and morphology properties

The crystal structures of the samples were characterized by X-ray powder diffraction (XRD). Fig. 1 depicts the XRD pattern of the prepared In_2S_3 nanoparticle. The obtained diffraction peaks were matched very well with the JCPDS Card No.: 00-032-0456 indicating the cubic β-In_2S_3. The diffraction peaks at $2\theta = 27.6^\circ$ (2 2 0), 32.1° (3 1 1), 38.9° (4 0 0), 51.3° (5 1 1), 56.3° (4 4 0), 66.3° (5 3 3), and 70.5° (4 4 4) were all corresponds to the lattice plane of only β-In_2S_3. No characteristic peaks were observed for the other impurities such as In_2O_3, S, or $In(OH)_3$, which confirmed that In_2S_3 was pure β-In_2S_3 nanoparticle. In Fig. 1, it can also be seen that the three sharp and more intense peaks (32.1°, 38.9°, 56.3°) indicate that the product is well crystallized and the crystal structure is very perfect. The crystallite sizes were calculated from the broadening of the diffraction (4 4 0) peaks using Scherrer's formula.

$$D = \frac{K\lambda}{\beta \cos\theta} \tag{1}$$

where D is the crystallite size (nm), K is the shape constant (0.89), λ is the wave length of CoKa radiation (0.178901 nm), θ is the diffraction angle (°), and β is the full width at half maximum (rad). The crystallite size of In_2S_3 was found to be 22 nm. The obtained result suggests that the synthesis method resulted in nanosized In_2S_3 particles.

The morphologies and size of the prepared In_2S_3 photocatalyst were investigated by SEM and TEM. Morphologies of the pure β-In_2S_3 nanoparticles were shown in Fig. 2. The crystallite nature of β-In_2S_3 was clearly observed from the Fig. 3 and the particles were

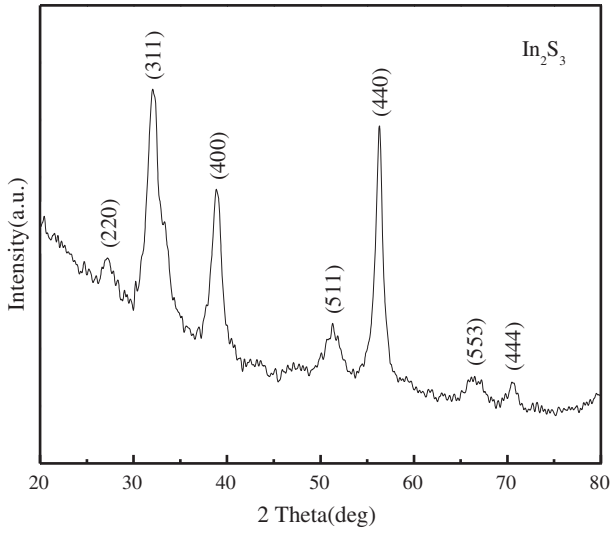

Fig. 1. XRD diffraction pattern of In_2S_3.

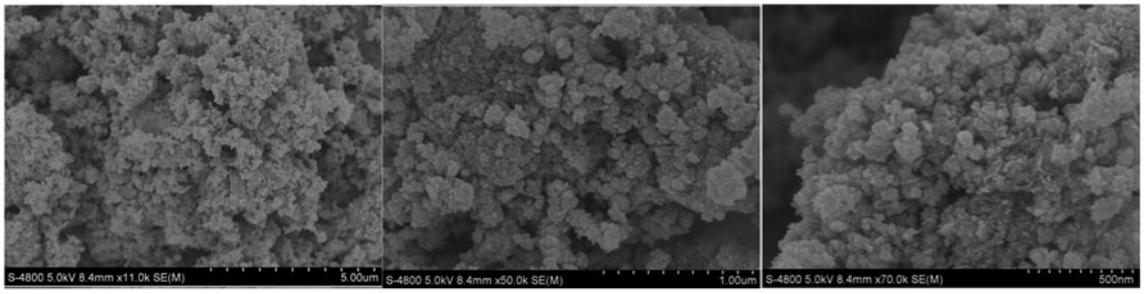

Fig. 2. SEM images of In_2S_3.

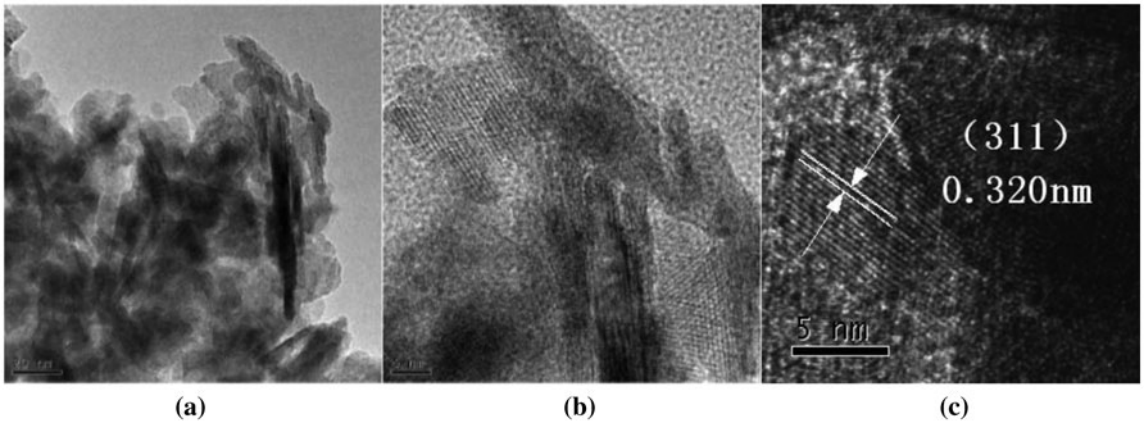

Fig. 3. TEM images of In_2S_3.

in uniform nanosheet. The observation of the catalyst confirms the uniform sized particles distributed homogeneously. SEM showed a higher particle size due to agglomeration of the nanoparticles. The actual size of In_2S_3 nanomaterials was measured using TEM images. TEM not only characterizes the morphology, but also gives crystallographic information of a material. A general view of the regions at the surface of the particles is shown in Fig. 3(a). It looks like a structure that consists of small sheets, of which contrasts are dark and light, respectively. Both of them are, in fact, the nanosheets oriented along different directions with respect to the electron beam. When the surface of the nanosheet is parallel to the electron beam it appears as dark contrast. On the contrary, the light contrast shows the surface of nanosheets. The observed various contrasts can be explained as a thickness effect, therefore, given by the combination of the different-oriented and overlapped nanosheets. Fig. 3(b) shows nanofiber-like regions embedded in the continuous nanosheet. It can be seen that the lattice fringes are continuous from the dark region to the nanosheet, indicating that both regions have the same lattice plane. The Fig. 3(c) image reveals the substructure of the nanosheets. The interfringe distance is measured to be 0.320 nm, which is close to the lattice space of (3 1 1) planes of β-In_2S_3. The obtained result was very well matched with the crystallite size measured by XRD analysis.

3.2. BET analysis

The surface area and porosity are important properties of a catalyst to determine its activity to apply for photocatalytic degradation applications. The pore architectures of the heterogeneous catalysts control the transport phenomena and govern the selectivity in various catalyzed reactions. The pore nature of In_2S_3 was confirmed by pore size distribution measurements, which was obtained by the nitrogen adsorption–desorption isotherm and BJH method. Fig. 4 shows the typical sorption isotherms and the corresponding pore size distribution (inset of Fig. 4) of In_2S_3. It is seen that the isotherm is type IV, indicating the presence of mesoporous materials (2–50 nm) according to the International Union of Pure and

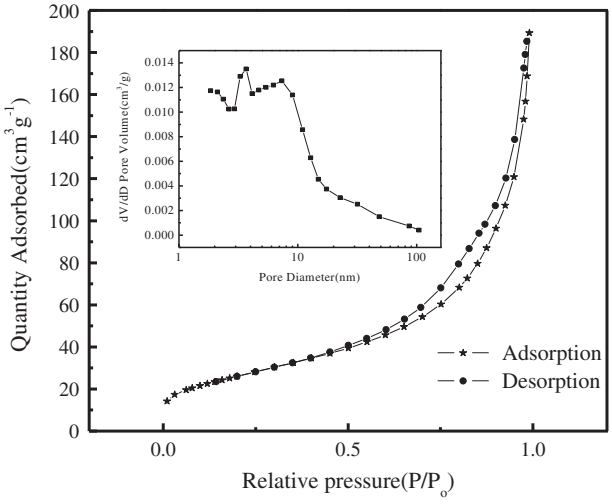

Fig. 4. N_2 adsorption and desorption isotherms and pore-size distribution (inset) for In_2S_3.

Applied Chemistry (IUPAC) classification. In general, mesoporous In_2S_3 having both high surface area and crystallinity possess good photocatalytic properties and employed for photocatalytic applications. The type-IV isotherm with a hysteresis loop (H3) in the range of 0.5–1.0 P/P_0 was obtained in the samples. According to the hysteresis loop, it can be seen that $P/P_0 = 0.99$, which indicates the presence of macropore (>50 nm). A quantitative calculation shows that the In_2S_3 samples possess a BET surface area of nearly 95.6726 m^2/g and a pore volume of 0.2932 $cm^3\ g^{-1}$. In addition, the average pore diameter, determined by Barrett–Joyner–Halenda (BJH) method using the desorption isotherm (inset of Fig. 4), was 10.4 nm. In addition, solar energy conversion efficiency may vary based on the particle size and pore size distribution [19]. At times, very small average pore size of β-In_2S_3 would hinder the access of organic pollutants resulting in poor degradation. Hence the β-In_2S_3 nanoparticles were experimented for its photocatalytic activity under the natural sunlight irradiation.

3.3. XPS analysis

Further evidence for the quality and composition of the samples was obtained by XPS of the products. Fig. 5 depicts the high resolution XPS spectra of In_2S_3. The XPS spectra showed the presence of In and S elements (Fig. 5(a)). The absence of the NO_3^- ion confirms the adopted washing procedure was more effective in the removal of the unwanted anion (NO_3^-) that may interfere with the photocatalytic activity. In addition, the C 1*s* peak in Fig. 5(a) was attributed to the adhesive tapes used to support the samples on the SEM platform or introduced from reactant thioacetamide. High-resolution core spectra of In 3*d* and S 2*p* of In_2S_3 are shown in panels b and c of Fig. 3, respectively. The In 3*d* spectrum (Fig. 5(b)) showed that the observed value of the binding energies for In $3d_{5/2}$ (444.8 eV) and In $3d_{3/2}$ (452.3 eV) was indicative of indium as trivalent In^{3+} ions. The observed value of the binding energies for In $3d_{5/2}$ (444.3 eV) agrees with the reported data in In_2S_3 (444.3 eV). These peaks are attributed to an active site which improves the photocatalytic activity, especially under the visible light irradiation [20]. The S 2*p* spectrum (Fig. 5(c)) appeared as a broad peak, which indicated that the particle surface sulfur might exist in form of S^{2-} (161.8 eV) and element S (163.8 eV). These values are in good agreement with the reported data.

The contents of In and S are quantified by In 3*d* and S 2*p* peak areas, and a molar ratio of 1:1.46 for In: S is given. However, there is a little inconsistency among the results, and this is very true for the stoichiometry of In_2S_3. No obvious peaks for elemental sulfur or other impurities were observed. Thus, the XPS results further proved that the sample was pure In_2S_3 and has no oxide impurities.

3.4. UV–vis absorption spectra and band gap energy

In addition to the structural properties, the optical properties of the In_2S_3 samples were also studied by UV–vis diffused reflectance spectroscopy (DRS). The DRS spectra of In_2S_3 samples were recorded in the wavelength range between 200 and 800 nm and are shown in Fig. 6. The obtained spectrum depicts the strong absorption of the prepared In_2S_3 both in the visible light spectrum and in the UV light region. It is clear that there is an absorption band at 280–370 and 600–640 nm, respectively. According to the characteristic step-like shape of the band, it should be attributed to the valence-to-conduction-band transition of electrons excitations in indium sulfide. The band structure indicates that charge transfer upon photoexcitation occurs from the S 3*p* orbital to the In 5*p* empty orbital. Kulbeka–Munk equation was used to obtain the accurate band gap energy of In_2S_3 nanoparticle. The reflectance data were converted to the absorption coefficient $F(R_\infty)$ values [21]:

$$F(R_\infty) = \frac{(1 - R_\infty)^2}{2R_\infty} \tag{2}$$

where R_∞ is the diffused reflectance of at the given wavelength.

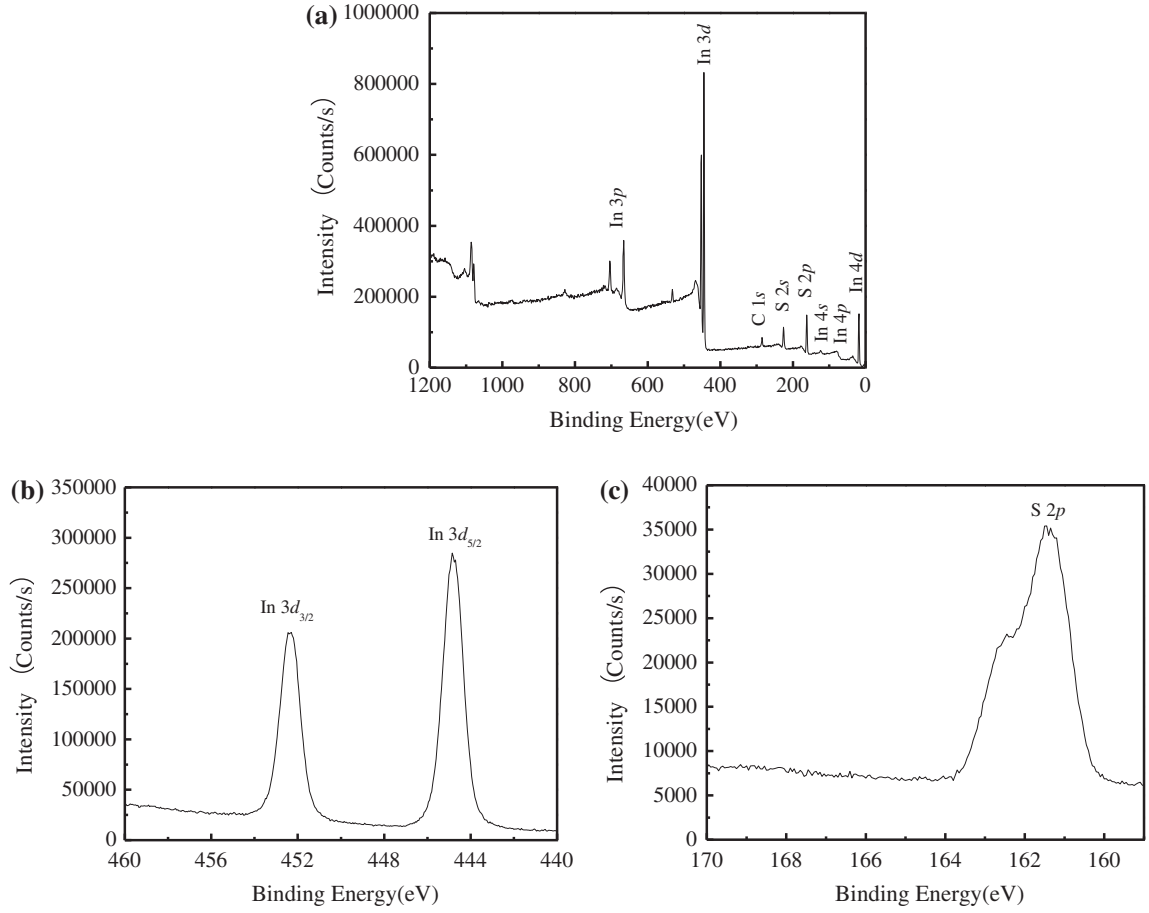

Fig. 5. XPS survey spectra of In_2S_3 samples: (a) survey spectra, (b) In 3*d* peak, and (c) S 2*p* peak.

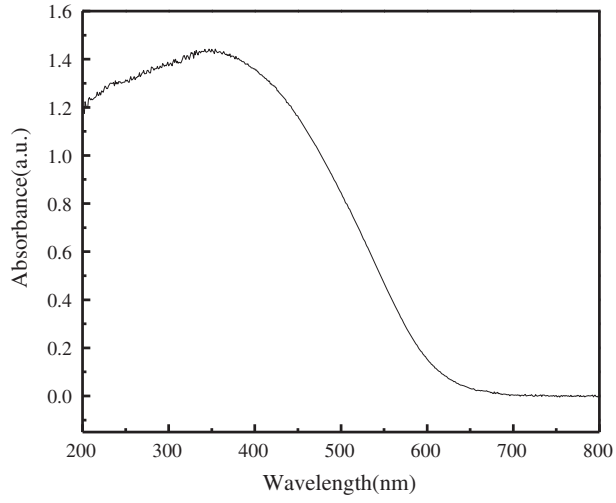

Fig. 6. UV–vis absorption of In_2S_3 photocatalyst.

$$E(\mathrm{eV}) = \frac{hC}{\lambda} \tag{3}$$

where h is the Planck's constant (4.14×10^{-15} eV s), C is the speed of light (3.0×10^{17} nms^{-1}), and λ is the wavelength (nm). From the Kulbeka–Munk analysis, the band gap energy of the prepared In_2S_3 was found to be 2.0 eV. Similar values of band gap energy were reported in the literature for In_2S_3 nanoparticle synthesized by different methods and different precursors [22].

To examine the quantum-confined effect of the products, UV–vis spectra is shown, when ethanol is used as a reference. The result of UV–vis spectroscopy (Fig. 6) shows that there is an absorption band at 280–370 nm. Because there is a strong influence from light scattering, the bumps they observe in UV–vis absorption may be difficult to discuss in terms of actual transitions. However, according to the characteristic step-like shape of the band, it should be attributed to the valence-to-conduction-band transition in indium sulfide. In bulk In_2S_3, the band gap (Eg) is reported to be between 2.00 and 2.20 eV with corresponding wavelengths from 620 to 550 nm.

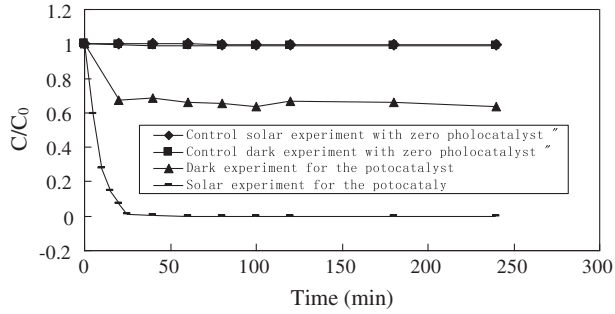

Fig. 7. Photocatalytic evaluation of the In_2S_3 photocatalyst under different conditions.

3.5. Photocatalytic activity

To study the photocatalytic activities of the β-In_2S_3 sample, antibiotic TC of low concentration was chosen as a model pollutant. The maximum absorptive energy of TC is at 357 nm.

The results of control experiments and photocatalytic degradation experiments in the optimal conditions [23] under the sunlight irradiation were depicted in Fig. 8. All the experimental data were statistically significant and the standard deviation was found to be less than 0.05. The obtained results suggests that a complete degradation of TC was achieved using the In_2S_3 photocatalyst with variation in time duration. The control experiments confirms that only a limited amount of TC was removed (<1%) in the absence of the In_2S_3 photocatalyst by direct photolysis. This demonstrates the high photocatalytic activity of the β-In_2S_3 under the sunlight. Moreover, the photocatalyst is quite stable. After four cycles run, slight decline in the photocatalytic activities was detected. From the dark reactions (see Fig. 7), it was clear that a modest removal of TC occurred due to adsorption (32–36%). Almost complete degradation (99–100%) was achieved for the catalyst under solar light radiation in 30 min.

3.6. Total organic carbon

The degree of mineralization of TC during the photocatalytic degradation was analyzed as a function of TOC and depicted in Fig. 8. In the figure, it can be seen that an efficiency of 69.53% was achieved for the In_2S_3 under the sunlight irradiation for 40 min. The removal efficiency of TOC was 60.71% in 20 min, and it tended be stable after 20 min. This indicated that TC could be mineralized by the In_2S_3 photocatalyst.

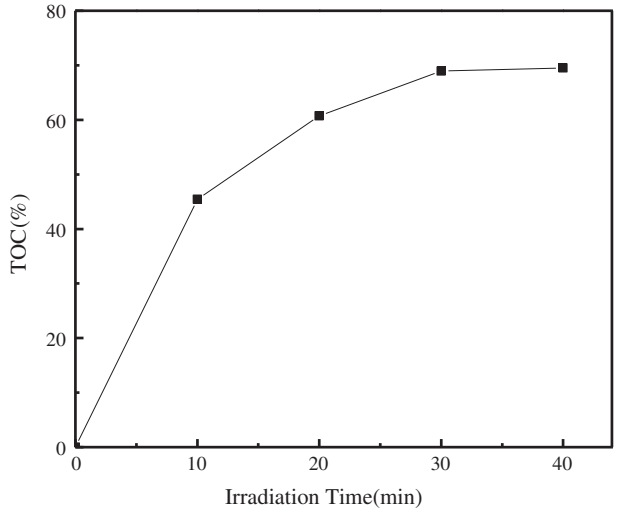

Fig. 8. Percentage mineralization of TC based on TOC analysis.

3.7. Kinetics of degradation

The degradation kinetics of TC on the In_2S_3 heterogeneous catalysts is explained by the first-order kinetics [24]. The first-order expression is given below:

$$-\ln\frac{C}{C_0} = k_1 t \tag{4}$$

where C_0 is the initial concentration of TC (mg L^{-1}) and C is the concentration TC at time t, and k_1 represents the rate constant of first-order reaction (min^{-1}).

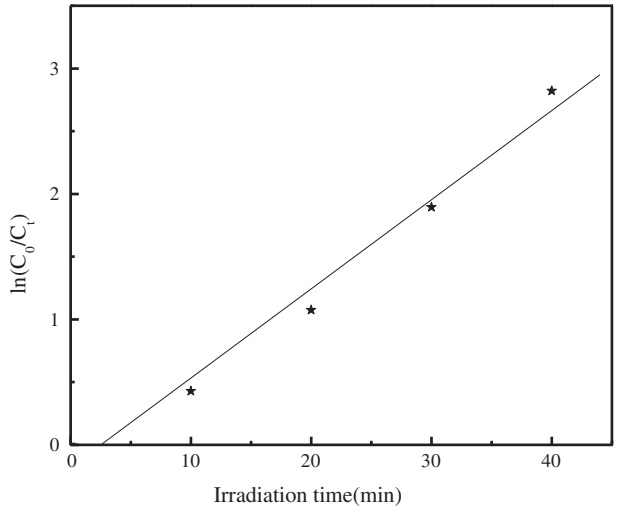

Fig. 9. The kinetics of TC degradation by prepared In_2S_3 photocatalyst.

The obtained experimental data were fitted with first-order kinetics and presented in Fig. 9. Higher correlation coefficients ($R^2 > 0.98$) obtained for the In_2S_3 photocatalyst indicates that the degradation of TC follows first-order kinetics. The first-order reaction rate constants (k_1) were found to be 0.071 min^{-1} for the In_2S_3. Higher rate constant value of the In_2S_3 indicates its potential for higher photocatalytic activity. The obtained results suggest that the higher photocatalytic activity of the In_2S_3 was attributed to the high crystallinity that increases the formation of hydroxyl radicals and super oxide radicals.

4. Conclusions

The present study exemplifies the successful synthesis of pure β-In_2S_3 nanoparticle through hydrothermal method. The structural and morphological studies confirmed that the In_2S_3 photocatalyst was in pure cubic phase. The In_2S_3 nanoparticle exhibited good crystallinity. The synthesized photocatalyst demonstrated an excellent photo response toward the sunlight irradiation by successfully degrading TC in shorter duration. The band gap energy of the In_2S_3 was found to be 2.0 eV. The higher photocatalytic activity of the In_2S_3 was attributed to good crystallinity that increases the formation of hydroxyl radicals and super oxide radicals. The kinetics of photocatalytic degradation confirms that the process follows the first-order kinetic pathway. This study provides a versatile approach of utilizing solar energy for complete degradation of antibiotic pollutant (TC) using pure β-In_2S_3 photocatalysts synthesized from In $(NO_3)_3$ precursor. Hence, the synthesized photocatalysts can be effectively used for water and wastewater treatment under solar light irradiation.

Acknowledgments

This work was supported by Fujian Provincial Key Laboratory of Photocatalysis-State Key Laboratory Breeding Base (038015) and funded by the Research Fund of Shaanxi Key Laboratory of Comprehensive Utilization of Tailings Resources (Shangluo University) (2014SKY-WK008, 2014SKY-WK005).

References

[1] P. Wang, B.B. Huang, Y. Dai, M.H. Whangbo, Plasmonic photocatalysts: Harvesting visible light with noble metal nanoparticles, Phys. Chem. Chem. Phys. 14 (2012) 9813–9825.

[2] E.I. Seck, J.M. Doña-Rodríguez, C. Fernández-Rodríguez, D. Portillo-Carrizo, M.J. Hernández-Rodríguez, O.M. González-Díaz, J. Pérez-Peña, Solar photocatalytic removal of herbicides from real water by using sol–gel synthesized nanocrystalline TiO_2: Operational parameters optimization and toxicity studies, Sol. Energy 87 (2013) 150–157.

[3] S. Khanchandani, S. Kundu, A. Patra, A.K. Ganguli, Band gap tuning of ZnO/In_2S_3 core/shell nanorod arrays for enhanced visible-light-driven photocatalysis, J. Phys. Chem. C 117 (2013) 5558–5567.

[4] X. Zhang, X.H. Li, C.L. Shao, J.H. Li, M.Y. Zhang, P. Zhang, K.X. Wang, N. Lu, Y.C. Liu, One-dimensional hierarchical heterostructures of In_2S_3 nanosheets on electrospun TiO_2 nanofibers with enhanced visible photocatalytic activity, J. Hazard. Mater. 260 (2013) 892–900.

[5] E. Dalas, L. Kobotiatis, Primary solid-state batteries constructed from copper and indium sulphides, J. Mater. Sci. 28 (1993) 6595–6597.

[6] M.Q. Yang, B. Weng, Y.J. Xu, Improving the visible light photoactivity of In_2S_3—Graphene nanocomposite via a simple surface charge modification approach, Langmuir 29 (2013) 10549–10558.

[7] B. Chai, T.Y. Peng, P. Zeng, J. Mao, Synthesis of floriated In_2S_3 decorated with TiO_2 nanoparticles for efficient photocatalytic hydrogen production under visible light, J. Mater. Chem. 21 (2011) 14587–14593.

[8] R. Nomura, S. Inazawa, K. Kanaya, H. Matsuda, Thermal decomposition of butylindium thiolates and preparation of indium sulfide powders, Appl. Organomet. Chem. 3 (1989) 195–197.

[9] P.G. Sheikhiabadi, M. Salavati-Niasari, F. Davar, Hydrothermal synthesis, characterization and optical properties of 3D flower like indium sulfide nanostructures, Superlattices Microstruct. 53 (2013) 76–88.

[10] P. Bera, S.I. Seok, Facile-chelating amine-assisted synthesis of β-In_2S_3 nanostructures from a new single-source precursor derived from *S*-methyl dithiocarbazate, J. Nanopart. Res. 13 (2011) 1889–1896.

[11] B. Yahmadi, N. Kamoun, R. Bennaceur, M. Mnari, M. Dachraoui, K. Abdelkrim, Structural analysis of indium sulphide thin films elaborated by chemical bath deposition, Thin Solid Films 473 (2005) 201–207.

[12] V.M. Anistchik, M.I. Markevich, F.A. Piskunov, V.A. Janushkevich, Laser induced synthesis of indium sulfides in a reactive liquid medium, Fiz. Khim. Obrab. Mater. 15 (1993) 35–37.

[13] K.H. Park, K. Jang, S.U. Son, Synthesis, optical properties, and self -assembly of ultrathin hexagonal In_2S_3 nanoplates, Angew. Chem. Int. Ed. 45 (2006) 4608–4612.

[14] S. Avivi (Levi), O. Palchik, V. Palchik, M.A. Slifkin, A.M. Weiss, A. Gedanken, Sonochemical synthesis of nanophase indium sulfide, Chem. Mater. 13 (2001) 2195–2200.

[15] W.D. Xiang, H.J. Zhao, J.S. Zhong, H.Y. Luo, X.L. Zhao, Z.P. Chen, X.J. Liang, X.Y. Yang, Synthesis and third-order optical nonlinearities of In_2S_3 quantum dots glass, J. Alloys Compd. 553 (2013) 135–141.

[16] N. Naghavi, R. Henriquez, V. Laptev, D. Lincot, Growth studies and characterisation of In_2S_3 thin films deposited by atomic layer deposition (ALD), Appl. Surf. Sci. 222 (2004) 65–73.

[17] L.Y. Chen, Z.D. Zhang, W.Z. Wang, Self-assembled porous 3D flowerlike β-In_2S_3 structures: Synthesis,

characterization, and optical properties, J. Phys. Chem. C 112 (2008) 4117–4123.
[18] S. Rengaraj, S. Venkataraj, C.W. Tai, Y. Kim, E. Repo, M. Sillanpää, Self-assembled mesoporous hierarchical-like In_2S_3 hollow microspheres composed of nanofibers and nanosheets and their photocatalytic activity, Langmuir 27 (2011) 5534–5541.
[19] K.P.S. Parmar, E. Ramasamy, J.W. Lee, J.S. Lee, A simple method for producing mesoporous anatase TiO_2 nanocrystals with elevated photovoltaic performance, Scr. Mater. 62 (2010) 223–226.
[20] A.A. Aziz, C.K. Cheng, S. Ibrahim, M. Matheswaran, P. Saravanan, Visible light improved, photocatalytic activity of magnetically separable titania nanocomposite, Chem. Eng. J. 183 (2012) 349–356.
[21] S. Valencia, J.M. Marín, G. Restrepo, Study of the bandgap of synthesized titanium dioxide nanoparticules using the sol-gel method and a hydrothermal treatment, J. Open Mater. Sci. 4 (2010) 9–14.
[22] N. Barreau, A. Mokrani, F. Couzinié-Devy, J. Kessler, Bandgap properties of the indium sulfide thin-films grown by co-evaporation, Thin Solid Films 517 (2009) 2316–2319.
[23] C.L. Ai, D.D. Zhou, Q. Wang, X.W. Shao, Y.J. Lei, Optimization of operating parameters for photocatalytic degradation of tetracycline using In_2S_3 under natural solar radiation, Sol. Energy 113 (2015) 34–42.
[24] K.V. Kumar, K. Porkodi, F. Rocha, Langmuir-Hinshelwood kinetics—A theoretical study, Catal. Commun. 9 (2008) 82–84.